Multiangle Imaging Spectroradiometer (MISR) global aerosol optical depth validation based on 2 years of coincident Aerosol Robotic Network (AERONET) observations

Ralph A. Kahn, Barbara J. Gaitley, John V. Martonchik, David J. Diner, and Kathleen A. Crean
Jet Propulsion Laboratory, California Institute of Technology, Pasadena, California, USA

Brent Holben
NASA Goddard Space Flight Center, Greenbelt, Maryland, USA

Received 27 February 2004; revised 13 May 2004; accepted 1 June 2004; published 9 March 2005.

[1] Performance of the Multiangle Imaging Spectroradiometer (MISR) early postlaunch aerosol optical thickness (AOT) retrieval algorithm is assessed quantitatively over land and ocean by comparison with a 2-year measurement record of globally distributed AERONET Sun photometers. There are sufficient coincident observations to stratify the data set by season and expected aerosol type. In addition to reporting uncertainty envelopes, we identify trends and outliers, and investigate their likely causes, with the aim of refining algorithm performance. Overall, about 2/3 of the MISR-retrieved AOT values fall within [0.05 or 20% × AOT] of Aerosol Robotic Network (AERONET). More than a third are within [0.03 or 10% × AOT]. Correlation coefficients are highest for maritime stations (~0.9), and lowest for dusty sites (more than ~0.7). Retrieved spectral slopes closely match Sun photometer values for Biomass burning and continental aerosol types. Detailed comparisons suggest that adding to the algorithm climatology more absorbing spherical particles, more realistic dust analogs, and a richer selection of multimodal aerosol mixtures would reduce the remaining discrepancies for MISR retrievals over land; in addition, refining instrument low-light-level calibration could reduce or eliminate a small but systematic offset in maritime AOT values. On the basis of cases for which current particle models are representative, a second-generation MISR aerosol retrieval algorithm incorporating these improvements could provide AOT accuracy unprecedented for a spaceborne technique.

Citation: Kahn, R. A., B. J. Gaitley, J. V. Martonchik, D. J. Diner, K. A. Crean, and B. Holben (2005), Multiangle Imaging Spectroradiometer (MISR) global aerosol optical depth validation based on 2 years of coincident Aerosol Robotic Network (AERONET) observations, *J. Geophys. Res.*, *110*, D10S04, doi:10.1029/2004JD004706.

1. Introduction

[2] Recent discoveries about the impact of airborne particles on regional radiation balance and water cycle [e.g., *Ramanathan et al.*, 2001] are adding significance to the well-established need for an accurate description of aerosols in global climate prediction models and in regional process studies [e.g., *Intergovernmental Panel on Climate Change* (*IPCC*), 2001; *Hansen et al.*, 1997]. Contributions from satellite aerosol products [e.g., *Remer et al.*, 2005; *Torres et al.*, 2002], surface measurements [e.g., *Dubovik et al.*, 2002], and aerosol transport models [e.g., *Tegen et al.*, 1997; *Chin et al.*, 2002] are helping create a global picture of aerosol distributions for these applications. The Multiangle Imaging Spectroradiometer (MISR) instrument is a player in this effort. One of its main goals is to produce frequent, global measurements of aerosol amount and type over a wide variety surface types, including key aerosol source regions, and to provide quantitative accuracy estimates for these values.

[3] MISR was launched into a Sun-synchronous polar orbit, crossing the equator at about 10:30 local time, in December 1999, aboard the NASA Earth Observing System's Terra satellite. It is among a new generation of satellite instruments, unique in having a combination of high spatial resolution, a wide range of along-track view angles, and high-accuracy calibration [*Diner et al.*, 1998]. Global coverage (to ±82° latitude) is obtained about once per week.

[4] MISR measures upwelling short-wave radiance from Earth in four spectral bands centered at 446, 558, 672, and 866 nm, at each of nine view angles spread out in the forward and aft directions along the flight path, at 70.5°, 60.0°, 45.6°, 26.1°, and nadir. Over a period of 7 min, as the spacecraft flies overhead, a 400-km-wide swath of Earth is

0148-0227/05/2004JD004706$09.00

successively viewed by each of MISR's nine cameras. As a result, the instrument samples a very large range of scattering angles, between about 60° and 160° at midlatitudes, providing information about aerosol microphysical properties [*Kahn et al.*, 1998, 2001a]. These views also capture air mass factors ranging from one to three, offering sensitivity to optically thin aerosol layers, and allowing aerosol retrieval algorithms to distinguish top-of-atmosphere reflectance contributions from the surface and atmosphere [*Martonchik et al.*, 1998, 2002].

[5] The MISR standard aerosol retrieval algorithm runs in an operational, fully automatic mode. It reports aerosol optical thickness (AOT) and aerosol type at 17.6 km resolution, by analyzing MISR top-of-atmosphere radiances from 16 × 16 pixel patches of 1.1-km resolution, [*Diner et al.*, 1999a]. On the basis of the prelaunch studies cited above, we expect MISR AOT sensitivity to vary with conditions. We predicted that at least over dark water, for AOT larger than about 0.1 at midvisible wavelengths, MISR aerosol type retrievals should exhibit particle size, shape, and some single-scattering albedo (SSA) sensitivity [*Kahn et al.*, 2001a]. These sensitivities, of interest in themselves, also reduce the MISR AOT retrieval's dependence on assumptions about particle microphysical properties.

[6] This paper aims at assessing how the early postlaunch version of the aerosol retrieval algorithm actually performs. It encompasses MISR level 2 aerosol products having version numbers from F03_0007 through F07_0015, available along with product descriptions and data handling tools from the NASA Langley Atmospheric Sciences Data Center (http://eosweb.larc.nasa.gov). A full chronology of algorithm changes is given on this Web site, by selecting "MISR data," then "data versioning," then "level 2 aerosol."

[7] Our approach is to compare coincident MISR AOT values with those obtained from 32 stations that are part of the Aerosol Robotic Network (AERONET). AERONET is a worldwide federation of ground-based, automated Sun photometers producing spectral AOT, aerosol microphysical properties, and precipitable water using standardized calibration, observation, cloud-clearing, data processing, and data distribution procedures [*Holben et al.*, 1998]. AERONET measurement uncertainties are well-understood [e.g., *Dubovik et al.*, 2000], and the data are widely used as a standard for satellite aerosol retrieval validation. Other MISR-AERONET AOT comparisons focus on southern Africa during August and September 2000 [*Diner et al.*, 2001], on the continental United States [*Liu et al.*, 2004], and on desert regions [*Martonchik et al.*, 2004; *Christopher and Wang*, 2004]. *Abdou et al.* [2005] studied cases where the Moderate resolution Imaging Spectroradiometer (MODIS) instrument, also aboard the Terra satellite, made observations coincident with MISR during 3 months of 2002.

[8] For this study, we selected 32 AERONET stations that capture four broad classes of aerosol air mass types over a 2-year period (Figure 1; Table 1). The data set provides adequate statistics for us to quantify uncertainties based on MISR-AERONET AOT differences, and to evaluate the way these differences depend on season and on expected aerosol type. We explore how patterns in the observed trends and outliers may relate to specific assumptions in the MISR algorithm, such as component particle properties and mixture definitions, surface boundary conditions, and cloud screening, with the goal of further refining the MISR aerosol retrieval algorithm itself.

[9] This paper is organized as follows: Section 2 describes how the MISR and AERONET data were selected and processed, and gives an overview of sampling statistics. In section 3 we identify trends and patterns in the AOT differences, stratified by expected aerosol type and season, investigate outliers, and explore possible causes for the observed behaviors. The final section summarizes the results and presents conclusions.

2. Data Selection and Analysis Approach

[10] AERONET direct-Sun measurements are taken automatically every 15 min by Sun- and sky-scanning CIMEL Sun photometers during daylight hours. Standard processing automatically generates AOT from direct transmission, calibrated using the Langley method, in bands centered at about 340, 380, 440, 500, 675, 870, and 1020 nm, along with column water vapor [*Holben et al.*, 1998].

[11] The MISR standard aerosol retrieval algorithm searches a data base of top-of-atmosphere (TOA) radiances simulated for the MISR channels, assuming a range of candidate aerosol mixtures and optical depths, and compares them with the observed radiance imagery [*Martonchik et al.*, 1998; *Diner et al.*, 1999a]. Component particle optical properties assumed in the early postlaunch MISR standard aerosol retrieval cover ranges of "small," "medium," and "large," nonabsorbing and absorbing, spherical and randomly oriented nonspherical types (Table 2). A limited selection of mixtures of these components is used in the retrievals, as given in Table 3. The MISR AOTs evaluated in this study are "regional mean" values, which are averages, with equal weight, of the AOT obtained for each mixture in the data base that yielded a successful retrieval. Aerosol retrieval success is measured by the degree to which observed multiangle, multispectral TOA radiances match modeled radiances, using several chi-squared criteria [e.g., *Kahn et al.*, 1998; *Martonchik et al.*, 1998, 2002].

[12] We worked with MISR and AERONET AOT data that met the cloud-free and other high-quality data standards set by the MISR and AERONET experiment teams, respectively. MISR level 2 aerosol retrievals use only data that pass angle-to-angle smoothness and spatial correlation tests [*Martonchik et al.*, 2002], as well as stereoscopically derived cloud masks and adaptive cloud-screening brightness thresholds [*Diner et al.*, 1999b; *Zhao and Di Girolamo*, 2004]. AERONET level 1.5 products are based on preobservation instrument calibrations, and AOT retrievals are performed only on cloud-screened data, based on low variability among three direct-Sun observations taken 1 min apart, on each 15-min measurement center [*Smirnov et al.*, 2000].

[13] We selected geographically diverse AERONET sites that provided generally good-quality measurement records, as well-populated as possible between December 2000 and November 2002. Most sites produced at least 12 months of data during this 24-month period. Among these sites, we identified seven or more locations dominated, at least during some seasons, by each of four aerosol air mass types:

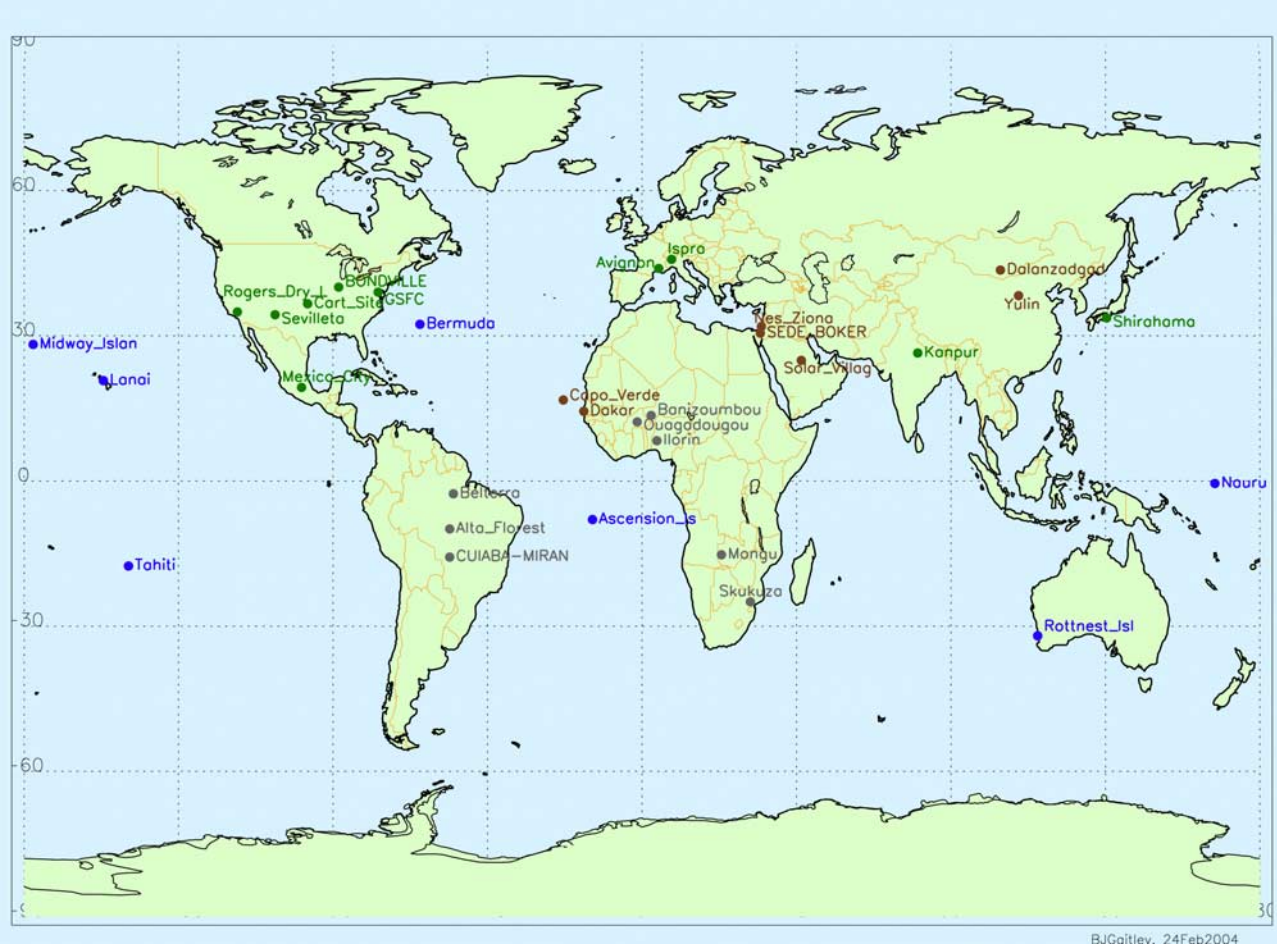

Figure 1. Geographical distribution of the 32 sites used in this study. Sites are color-coded according to expected aerosol air mass type: gray for biomass burning, green for continental, brown for dusty, and blue for maritime.

biomass burning, continental, dusty, and maritime (Table 1). Although component particle microphysical properties are known to vary within each category, these four groupings represent the broad classes of aerosols we expect to observe globally with MISR.

[14] We then searched the MISR level 2 standard aerosol product (version 12), for overflights having successful retrievals either in the MISR 17.6 km retrieval region containing each AERONET station selected (the "central" region), or in one or more of the eight retrieval regions surrounding the central one. We also required that the AERONET time series for each coincidence include at least one AOT retrieval during the hour before the MISR overpass, and at least one during the hour after the overpass. To facilitate comparisons, all AERONET AOT values used were interpolated linearly to the MISR band effective wavelengths.

[15] A fundamental difference between the MISR and AERONET AOT observations is that MISR acquires instantaneous data over an entire 20- to 50-km study area (one central + eight surrounding 17.6 km retrieval regions), whereas AERONET obtains a time series of point data at each surface station. For each event, we averaged with equal weight all available AERONET AOT retrievals for a 2-hour window centered on the MISR overpass time. This crudely covers the period during which aerosols advecting at 5–15 m/s would traverse the MISR study area, though not necessarily sampling it uniformly. We rely on the large number of events included in this study to average out any subtle sampling anomalies, and to highlight as outliers any individual pathological cases.

[16] Table 4 summarizes the sampling statistics for the entire data set, stratified by season, expected aerosol type, and central versus surrounding retrieval coincidence. MISR AOT retrievals obtained in the central 17.6 km retrieval region are preferentially used for comparisons. When there is no center region MISR retrieval for a given MISR-AERONET coincidence, the average of all available AOT retrievals in the eight surrounding regions is reported. These are book-kept separately, allowing us to crudely assess aerosol variability on 20- to 50-km scales, and to obtain better sampling in some categories.

[17] Over 2 years, we obtained 579 central events and 326 surroundings events having coincident MISR-AERONET observations that met the data selection criteria. There are over 130 central events for each of biomass burning, continental, and dusty aerosol types, and about 30 or more in each seasonal subcategory. This means approximately

Table 1. AERONET Validation Sites Used in This Study[a]

Site Name	Latitude	Longitude	Altitude, m	AERONET Data Availability, December 2000 and November 2002	Available Months
			Biomass Burn		
Alta_Floresta	−9.92	−56.02	175	gaps: Dec. 2000; Jan.–March, Nov.–Dec. 2001; March 2002	17
Banizoumbou	13.53	2.67	250	gaps: March–May, July 2001; May–June 2002	18
Belterra	−2.65	−54.95	70	data: July–Aug., Oct.–Dec. 2001; Jan., Sept.–Oct. 2002	8
Cuiaba-Miranda	−15.72	−56.02	210	data: June–Oct. 2001; Sept.–Oct. 2002	7
Ilorin	8.32	4.33	350	data: Jan.–May, Oct. 2001	6
Mongu	−15.25	23.15	1107	gaps: Feb., Nov. 2001	22
Ouagadougou	12.18	−1.38	290	gaps: Aug.–Sept. 2001; May–Oct. 2002	16
Skukuza	−24.98	31.58	150	gaps: Nov.–Dec. 2001	22
			Continental		
Avignon	43.92	4.87	32	gap: Dec. 2001	23
Bondville	40.05	−88.37	212	gaps: Dec. 2000; Feb., July, Nov. 2001; March, July–Aug. 2002	17
Cart_Site	36.60	−97.40	315	gaps: Dec. 2000; March–April, Oct.–Nov. 2002	19
GSFC	39.02	−76.87	50	gap: June–July 2001	22
Ispra	45.80	8.62	235	gaps: Dec. 2000; Jan., March–April, Nov. 2001; Nov. 2002	18
Kanpur	26.43	80.33	142	gaps: Dec. 2000; Jan., July–Sept. 2001; Aug.–Sept. 2002	18
Mexico_City	19.33	−99.17	2268	gaps: July–Dec. 2001; June–Nov. 2002	12
Rogers Dry Lake	34.92	−117.88	680	gaps: Nov.–Dec. 2001; Sept. 2002	21
Sevilleta	34.35	−106.88	1477	gaps: Dec. 2000; Jan., Sept., Dec. 2001; Jan., April, Aug., Nov. 2002	16
Shirahama	33.68	135.35	10	data: Dec. 2000; Dec. 2001; Jan., March, May–July, Sept. 2002	8
			Dusty		
Capo_Verde	16.72	−22.93	60	gaps: May 2001; March–April, July, Nov. 2002	19
Dakar	14.38	−16.95	0	data: Dec. 2000; Jan.–Aug. 2001; March 2002	10
Dalanzadgad	43.57	104.42	1470	gaps: Dec. 2000; Jan., March–May, July–Sept. 2001; April, June–Aug. 2002	11
Nes_Ziona	31.92	34.78	40	gaps: Sept.–Dec. 2001; Jan.–Feb., April, Sept.–Nov. 2002	15
Sede_Boker	30.52	34.47	480	gaps: Dec. 2000; May–Nov. 2001; Feb.–Aug. 2002	9
Solar_Village	24.90	46.40	650	gaps: Dec. 2000; Feb., Oct.–Dec. 2001; Feb.–March, June, Aug., Oct. 2002	14
Yulin	38.27	109.72	1080	gaps: Dec. 2000; Jan.–April, July, Dec. 2001; Jan.–March, Nov. 2002	13
			Maritime		
Ascension_Island	−7.97	−14.40	30	data: Dec. 2000; Jan.–Feb. 2001; Feb., May–July, Sept. 2002	8
Bermuda	32.37	−64.68	10	gaps: Dec. 2000; Jan., March, Nov.–Dec. 2001; Jan.–Feb., April, Nov. 2002	15
Lanai	20.82	−156.93	80	gaps: Dec. 2000; Dec. 2001; April, July–Nov. 2002	16
Midway Island	28.20	−177.37	0	data: Feb., April–Sept., Dec. 2001; Jan. 2002	9
Nauru	−0.52	166.90	7	data: Aug.–Oct. 2001	3
Rottnest Island	−32.00	115.28	40	gaps: Dec. 2000; Jan.–Feb., Aug.–Oct. 2001, May–June, Oct.–Nov. 2002	14
Tahiti	−17.57	−149.60	98	data: March, July–Sept. 2001	4

[a]Available months refers to the number of months for which AERONET data are available during the study period.

Table 2. MISR Early Postlaunch Component Aerosol Optical Models[a]

Number	Component Name	r_1, μm	r_2, μm	r_c, μm	r_e, μm	σ	SSA (446)	SSA (558)	SSA (672)	SSA (866)	AOT(446)/ AOT(558)	AOT(672)/ AOT(558)	AOT(867)/ AOT(558)	g (558)	Particle Size/ Shape Category
1	sph_nonabsorb_0.06	0.001	0.4	0.03	0.06	1.65	1.00	1.00	1.00	1.00	1.95	0.55	0.23	0.352	small spherical
2	sph_nonabsorb_0.12	0.001	0.75	0.06	0.12	1.7	1.00	1.00	1.00	1.00	1.54	0.66	0.35	0.609	small spherical
3	sph_nonabsorb_0.26	0.01	1.5	0.12	0.26	1.75	1.00	1.00	1.00	1.00	1.18	0.82	0.58	0.717	medium spherical
4	sph_nonabsorb_0.57	0.01	4	0.24	0.57	1.8	1.00	1.00	1.00	1.00	0.98	0.99	0.91	0.722	large spherical
5	sph_nonabsorb_1.28	0.01	8	0.5	1.28	1.85	1.00	1.00	1.00	1.00	0.96	1.04	1.10	0.728	large spherical
6	nonsph_absorb_1.18_lo	0.05	2	0.47	1.18	2.6	0.805	0.880	0.914	0.980	0.97	1.03	1.08	0.730	medium dust low
7	nonsph_absorb_1.18_hi	0.05	2	0.47	1.18	2.6	0.805	0.880	0.914	0.980	0.97	1.03	1.08	0.730	medium dust high
8	nonsph_absorb_7.48	0.5	15	1.9	7.48	2.6	0.612	0.694	0.734	0.900	1.00	1.00	1.00	0.881	coarse dust
9	sph_absorb_0.04	0.001	0.5	0.012	0.04	2.0	0.250	0.209	0.172	0.123	1.37	0.77	0.54	0.337	black carbon

[a]These aerosol optical models apply to the MISR standard level 2AS aerosol product, versions F03_0007 through F07_0015. A number-weighted log-normal particle size distribution function is adopted for all components. Single scattering properties were calculated using a Mie code for the spherical particles; the dust component properties were calculated using the T-matrix method for a mixture of oblate and prolate ellipsoids having a uniform distribution of aspect ratios [*Mishchenko et al.*, 1997]. Wavelength in nm is specified in parentheses where appropriate. Here r_1 and r_2 are the upper and lower limits of the size distribution; r_c, r_e, and σ are the characteristic radius, effective radius, and width parameters in the log-normal distribution; and SSA is the single-scattering albedo. The asymmetry parameter (g) will generally represent particle scattering phase functions poorly for the purpose of calculating MISR multiangle radiances and is given here only in MISR green band for reference; full phase functions are available in the MISR standard product "ACP_APOPP" files. All spherical components are assumed to be distributed vertically within 10 km of the surface and have scale heights of 2 km. Medium dust (nonsph_absorb_1.18_lo) is confined to the lowest 5 km, and coarse dust (nonsph_absorb_7.48) is confined to the lowest 2 km. Transported mineral dust (nonsph_absorb_1.18_hi) resides between 5 and 10 km of the surface and has a 10-km scale height.

Table 3. MISR Early Postlaunch Aerosol Mixture Properties[a]

		Fraction of AOT(558) in Component										
Number	Type	1	2	3	4	5	6	7	8	9	SSA (558)	A_λ
1	spherical small clean	1.0	-	-	-	-	-	-	-	-	1.00	3.22
2	spherical small clean	0.5	0.5	-	-	-	-	-	-	-	1.00	2.71
3	spherical small clean	-	1.0	-	-	-	-	-	-	-	1.00	2.24
4	spherical small clean	-	0.5	0.5	-	-	-	-	-	-	1.00	1.63
5	spherical medium clean	-	-	1.0	-	-	-	-	-	-	1.00	1.09
6	spherical medium clean	-	-	0.5	0.5	-	-	-	-	-	1.00	0.56
7	spherical medium clean	-	-	-	1.0	-	-	-	-	-	1.00	0.10
8	spherical medium clean	-	-	-	0.5	0.5	-	-	-	-	1.00	−0.05
9	spherical bimodal clean	-	0.5	-	-	0.5	-	-	-	-	1.00	0.82
10	spherical bimodal clean	0.5	-	-	-	0.5	-	-	-	-	1.00	1.19
11	spherical small dirty	0.85	-	-	-	-	-	-	-	0.15	0.88	2.87
12	spherical small dirty	0.45	0.4	-	-	-	-	-	-	0.15	0.88	2.50
13	spherical small dirty	-	0.85	-	-	-	-	-	-	0.15	0.88	2.09
14	spherical small dirty	-	0.45	0.4	-	-	-	-	-	0.15	0.88	1.62
15	spherical medium dirty	-	-	0.85	-	-	-	-	-	0.15	0.88	1.13
16	spherical medium dirty	-	-	0.45	0.4	-	-	-	-	0.15	0.88	0.71
17	spherical medium dirty	-	-	-	0.85	-	-	-	-	0.15	0.88	0.29
18	dusty low	-	-	0.75	-	-	0.25	-	-	-	0.97	0.72
19	dusty low	-	-	0.5	-	-	0.5	-	-	-	0.94	0.40
20	dusty low	-	-	0.25	-	-	0.75	-	-	-	0.91	0.13
21	dusty low	-	-	-	-	-	1.0	-	-	-	0.88	−0.11
22	dusty low	-	-	-	-	-	0.75	-	0.25	-	0.83	−0.08
23	dusty low	-	-	-	-	-	0.5	-	0.5	-	0.79	−0.06
24	dusty high	-	-	-	-	-	-	1.0	-	-	0.88	−0.11

[a]Aerosol component optical models are described in Table 2; components 1–5 are spherical nonabsorbing, 6–7 are medium dust, 8 is coarse dust, and 9 is a soot analog. "A_λ." is the angstrom exponent, calculated as the slope of the least squares fit line to the logarithm of the spectral AOT versus wavelength; larger particles generally produce smaller (or negative) A_λ.

20% of overpasses resulted in coincident, cloud-free, central AOT comparisons. Maritime cases are sampled about half as often as the other categories, due in part to data gaps; during the 2-year study period, remote island stations at Nauru, Tahiti, Ascension, and Midway Islands obtained data for only 3, 4, 8, and 9 months, respectively (Table 1). Frequent cloud contamination also contributes to lower sampling at the maritime sites. In most categories, the surroundings retrievals increase the number of coincident events by 50–100%.

[18] Also shown in Table 4 are the numbers of events in each category for which the best fitting aerosol mixture in the MISR version 12 retrieval contained (1) only spherical, nonabsorbing particles, (2) both spherical absorbing and nonabsorbing particles, or (3) both nonspherical mineral dust and spherical nonabsorbing particles. (These correspond to mixtures 1–10, 11–17, and 18–24, respectively, in Table 3.) Although the best fitting mixture is generally unique, more than one mixture can meet the chi-squared criteria for a successful retrieval; "regional mean AOT," the primary MISR product evaluated in this study, is the average of the AOT retrieved for all successful mixtures. These data are discussed in section 3.

3. Results

[19] Figure 2 shows scatterplots of MISR versus AERONET green band AOT for all central coincidences, stratified by expected aerosol air mass type. Regression statistics for central and surroundings cases, and for all four MISR spectral bands, are given in Table 5. Most of the green band AOT values fall below 0.4 for the biomass burning, continental, and dusty categories; for maritime, nearly all are below 0.2, as expected. Spectral behavior also agrees qualitatively with expectation; MISR AOT decreases systematically with increasing wavelength (Table 5), and the distributions of clusters and outliers in the blue, red, and near-infrared bands (not shown) are similar to those for the green band in all categories (Figure 2).

Table 4. Total and Seasonal Sampling Statistics, 2001–2002[a]

	Total	DJF	MAM	JJA	SON
Biomass Burning					
Central	135	31	29	46	29
Surrounding	59	13	16	17	13
Best fit nonabsorbing	66	20	13	14	19
Best fit absorbing	41	1	8	27	5
Best fit dusty	28	10	8	5	5
Continental					
Central	247	46	77	72	52
Surrounding	123	34	30	17	42
Best fit nonabsorbing	191	41	52	50	48
Best fit absorbing	44	4	18	18	4
Best fit dusty	12	1	7	4	0
Dusty					
Central	132	28	40	33	31
Surrounding	77	23	15	12	27
Best fit nonabsorbing	78	15	22	21	20
Best fit absorbing	28	8	7	6	7
Best fit dusty	26	5	11	6	4
Maritime					
Central	65	16	19	19	11
Surrounding	67	13	15	22	17
Best fit nonabsorbing	32	5	8	13	6
Best fit absorbing	27	8	10	5	4
Best fit dusty	4	2	1	0	1

[a]DJF, December, January, and February (northern winter); MAM, March, April, and May (northern spring); JJA, June, July, and August (northern summer); SON, September, October, and November (northern autumn).

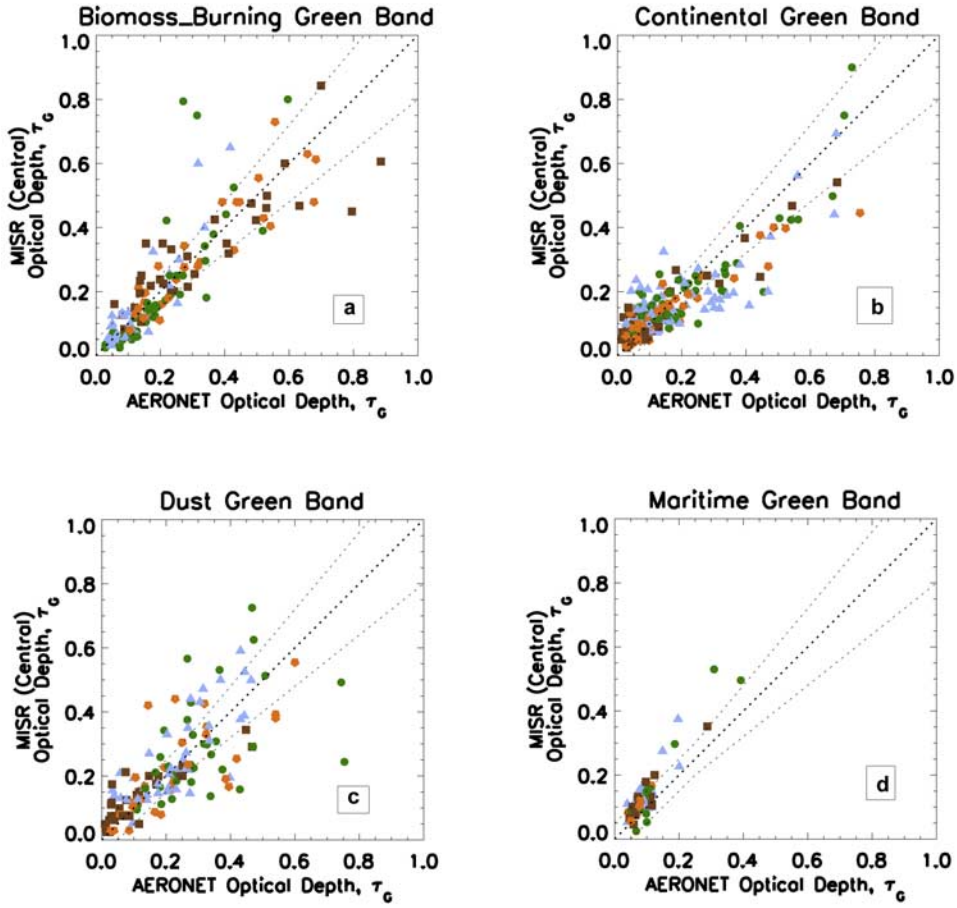

Figure 2. Scatterplots giving MISR green-band AOT comparisons for 579 central MISR-AERONET coincidences. These represent all such events between December 2000 and November 2002 at 32 sites. The plots are stratified by expected aerosol air mass type: (a) biomass burning, (b) continental, (c) dusty, and (d) maritime. The dashed lines are the 1:1 line and the envelope of ±0.05 or 20% × AOT, whichever is larger. Symbols and colors indicate season: DJF (northern winter), brown squares; MAM, blue triangles; JJA, green circles; SON, orange pentagons. Occasional extreme outliers are plotted beyond the axes.

[20] MISR and AERONET AOT values are well-correlated; the correlation coefficients exceed 0.8 in all categories except central dusty, where they are still larger than 0.72 (Table 5). Formally, the standard deviation of the MISR (central)-AERONET midvisible AOT differences, for all points having MISR AOT below 0.5, is between 0.07 and 0.08 for biomass burning and continental sites, around 0.1 for dusty sites, and below 0.04 for maritime. Generally, the magnitude of the AOT discrepancy scales as the AOT itself in all categories, and amounts to a scatter of between 30% and 54%, depending on category. Sixty-three percent of the MISR AOT values fall within [0.05 or 20% × AOT] of the AERONET results, whichever is larger (dashed lines in Figure 2), which agrees with our prelaunch estimate for MISR AOT accuracy [*Kahn et al.*, 1998]. The early post-launch MISR algorithm places 40% of the values within [0.03 or 10% × AOT] of AERONET. These percentages do not vary much among the aerosol type categories, though they are slightly higher for maritime cases, which have lower AOT, and are slightly lower for dusty cases, which have higher AOT (Table 5).

[21] Looking in more detail at Figure 2, data points scatter fairly uniformly about the 1:1 line for biomass burning and dusty sites, whereas for continental cases, MISR AOT is generally lower, and for maritime, it is almost always higher. Regression line slopes quantify this pattern; they are smallest for continental sites and highest for maritime. MISR-AERONET deviations for maritime cases are always greater than zero in the available data; for biomass burning and dusty sites, deviations are also more frequently biased high, but lower values are far more common than for maritime events.

[22] The comparison between statistics for "central" and "surroundings" cases combines sampling and spatial variability effects. Regression line slopes, intercepts, and correlation coefficients at biomass burning and continental sites for the surroundings are close to the central values, and AOT difference standard deviations are greater for the surroundings. This behavior might be expected if aerosol amount and other properties vary gradually on 10- to 50-km scales (Table 5; *Anderson et al.* [2003]). For maritime sites, the surroundings correlation coefficients are lower, but

Table 5. MISR Mean AOT and MISR-AERONET Comparison Statistics by Aerosol Type, 2001–2002

	MISR Mean AOT[a]	AERONET Mean AOT[a]	Mean AOT Difference,[b] %	Standard Deviation (AOT Difference)[c]	Correlation Coefficient	Regression Slope (Gain)[a]	Regression Y-Intercept (Offset)[a]	Value Within 0.05 or 20%, %	Value Within 0.03 or 10%, %
Biomass Burning									
Central, 135 cases								66	39
Blue	0.310 ± 0.112	0.300 ± 0.016	28	0.081	0.858	0.866 ± 0.003	0.050 ± 0.001		
Green	0.246 ± 0.101	0.243 ± 0.013	32	0.071	0.845	0.896 ± 0.003	0.028 ± 0.001		
Red	0.201 ± 0.091	0.195 ± 0.011	38	0.064	0.843	0.923 ± 0.004	0.021 ± 0.001		
NIR	0.152 ± 0.082	0.152 ± 0.010	45	0.058	0.832	0.900 ± 0.004	0.015 ± 0.001		
Surrounding, 59 cases								56	32
Blue	0.384 ± 0.125	0.378 ± 0.026	37	0.103	0.862	0.853 ± 0.006	0.061 ± 0.001		
Green	0.296 ± 0.108	0.307 ± 0.022	40	0.084	0.853	0.851 ± 0.006	0.035 ± 0.000		
Red	0.237 ± 0.097	0.247 ± 0.019	47	0.072	0.846	0.841 ± 0.006	0.029 ± 0.000		
NIR	0.175 ± 0.089	0.198 ± 0.017	58	0.065	0.826	0.760 ± 0.006	0.025 ± 0.000		
Continental									
Central, 247 cases								63	42
Blue	0.206 ± 0.068	0.208 ± 0.018	52	0.089	0.884	0.683 ± 0.004	0.064 ± 0.000		
Green	0.154 ± 0.059	0.162 ± 0.014	54	0.076	0.870	0.681 ± 0.004	0.044 ± 0.000		
Red	0.121 ± 0.053	0.122 ± 0.011	68	0.066	0.851	0.683 ± 0.004	0.038 ± 0.000		
NIR	0.088 ± 0.047	0.089 ± 0.008	70	0.055	0.816	0.704 ± 0.004	0.025 ± 0.000		
Surrounding, 123 cases								69	42
Blue	0.207 ± 0.087	0.211 ± 0.017	51	0.109	0.867	0.693 ± 0.007	0.061 ± 0.000		
Green	0.159 ± 0.071	0.17 ± 0.014	52	0.091	0.875	0.693 ± 0.007	0.041 ± 0.000		
Red	0.127 ± 0.062	0.135 ± 0.011	68	0.08	0.870	0.679 ± 0.007	0.036 ± 0.000		
NIR	0.094 ± 0.057	0.105 ± 0.009	60	0.071	0.824	0.638 ± 0.007	0.027 ± 0.000		
Dusty									
Central, 132 cases								55	37
Blue	0.285 ± 0.106	0.258 ± 0.019	46	0.107	0.751	0.733 ± 0.004	0.096 ± 0.001		
Green	0.228 ± 0.099	0.226 ± 0.016	52	0.104	0.728	0.693 ± 0.004	0.072 ± 0.001		
Red	0.187 ± 0.092	0.198 ± 0.014	62	0.098	0.717	0.669 ± 0.004	0.055 ± 0.000		
NIR	0.142 ± 0.075	0.159 ± 0.012	108	0.079	0.745	0.707 ± 0.004	0.030 ± 0.000		
Surrounding, 77 cases								56	38
Blue	0.315 ± 0.116	0.273 ± 0.016	43	0.084	0.828	1.077 ± 0.003	0.020 ± 0.001		
Green	0.257 ± 0.111	0.242 ± 0.014	40	0.088	0.810	1.000 ± 0.002	0.016 ± 0.001		
Red	0.216 ± 0.105	0.214 ± 0.013	46	0.092	0.791	0.907 ± 0.002	0.021 ± 0.001		
NIR	0.168 ± 0.080	0.175 ± 0.011	62	0.068	0.835	0.900 ± 0.002	0.010 ± 0.000		
Maritime									
Central, 65 cases								69	45
Blue	0.177 ± 0.060	0.110 ± 0.007	73	0.059	0.860	1.376 ± 0.011	0.026 ± 0.001		
Green	0.137 ± 0.037	0.098 ± 0.007	47	0.038	0.916	1.381 ± 0.013	0.001 ± 0.001		
Red	0.108 ± 0.030	0.083 ± 0.006	40	0.031	0.918	1.317 ± 0.014	−0.001 ± 0.001		
NIR	0.076 ± 0.021	0.068 ± 0.006	34	0.021	0.919	1.081 ± 0.013	0.003 ± 0.001		
Surrounding, 67 cases								73	49
Blue	0.153 ± 0.045	0.098 ± 0.009	77	0.046	0.719	0.891 ± 0.011	0.065 ± 0.001		
Green	0.122 ± 0.036	0.09 ± 0.008	54	0.037	0.748	0.905 ± 0.012	0.041 ± 0.001		
Red	0.100 ± 0.032	0.077 ± 0.007	54	0.033	0.738	0.919 ± 0.015	0.030 ± 0.001		
NIR	0.075 ± 0.029	0.064 ± 0.007	55	0.030	0.692	0.771 ± 0.016	0.026 ± 0.001		

[a]The AERONET AOT uncertainty is obtained as follows: For each event the standard deviation of all AERONET AOT values in the 2-hour time interval surrounding the MISR overpass is calculated; each event is treated as independent, so the root-sum-squared of these standard deviations, for all events in the category, is reported. The uncertainty estimate for MISR AOT is obtained assuming AERONET as truth, so MISR AOT error for each event is the deviation of the MISR retrieved AOT from the MISR-AOT versus AERONET AOT regression line. The root-sum-squared of these deviations, for all events in the category, is reported. MISR AOT errors would be a factor 5–10 lower than those reported here, comparable to the AERONET AOT estimated from the time series, if they were instead estimated from variability in the retrievals themselves, either from AOT values for the range of mixtures that pass the algorithm criteria, or from spatial variability. Uncertainties in the linear-fit gains and offsets are calculated assuming the uncertainty in the AOT for each data point is the standard deviation of retrieved MISR AOT for all aerosol mixtures that meet the algorithm success criteria at that point.

[b]The mean AOT difference is the average value of ABS ((MISR-AERONET)/AERONET), expressed as a percent, where MISR and AERONET are AOT evaluated in each MISR spectral band. A single event, for which the AERONET AOT is extremely low, is responsible for the high mean AOT difference value of 108% for the central dusty near-infrared spectral band. Eliminating this event reduces the value to 84%.

[c]Events having AOT higher than 0.5 are rare in this data set. The standard deviation of MISR-AERONET AOT differences is calculated only over cases having $AOT_{MISR} < 0.5$, to avoid skewing this statistic with individual extreme outliers.

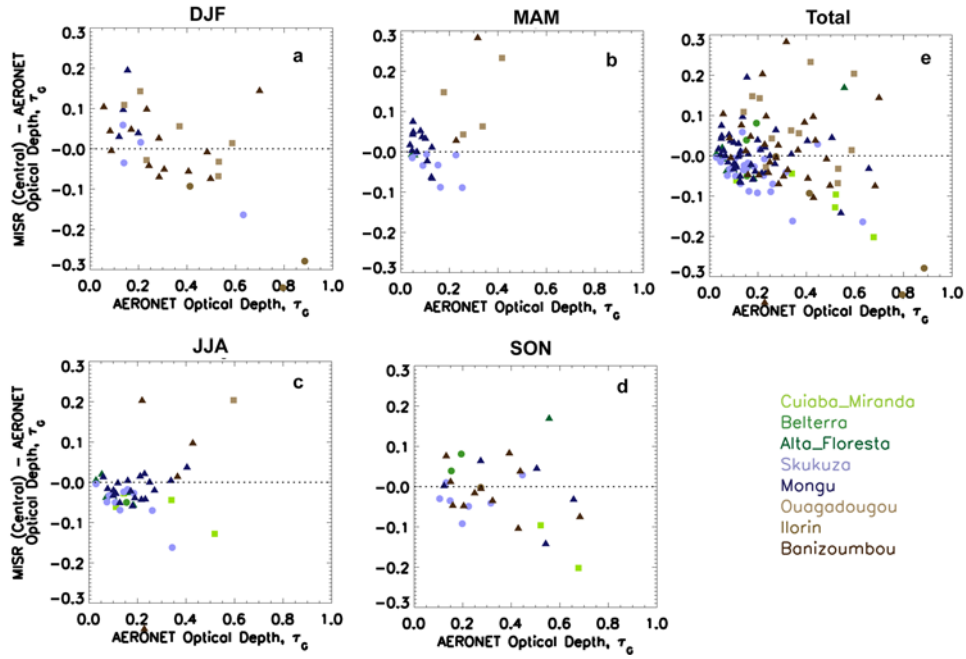

Figure 3. Biomass burning difference plots for 135 central coincidences at seven sites during the 2-year study period. Each plot shows the MISR-AERONET AOT difference at 558 nm wavelength, as a function of AERONET AOT. (a) Subset of all central events occurring during northern winter (December, January, and February). (b) Events occurring during northern spring (March, April, and May). (c) Events occurring during northern summer (June, July, and August). (d) Events occurring during northern autumn (September, October, and November). (e) All 135 events. Events are color-coded by site, as defined in the lower right: shades of green for South American sites, blues for southern African sites, and browns for northern African sites.

outliers affect the regression characteristics. At the dusty sites, the AOT discrepancy patterns are location-dependent; to interpret them we will look in more detail than is allowed by the Table 5 summary statistics.

[23] Beyond these generalizations, MISR-AERONET AOT difference patterns in Figure 2 appear to be dominated by site-specific effects. An inadequate selection of particle optical models in the early postlaunch MISR retrieval algorithm is likely to be a contributing factor; over ocean, assumed surface reflectivity behavior may be involved as well. In general, the MISR-retrieved AOT is boosted artificially if the algorithm chooses particles having single-scattering albedo (SSA) too low, or, over ocean, if it assumes a surface that is too dark. Thin, uniform cirrus is not included in the early postlaunch aerosol component suite (Table 2). Undetected by either instrument, thin cirrus could produce high AOT values for both AERONET and MISR. Since cirrus particles can be large relative to typical aerosols, they can produce larger forward scattering peaks, and the AERONET extinction estimate could be skewed low, producing a positive MISR-AERONET AOT difference. The magnitude of this effect depends on cirrus particle size and shape, and the fraction of optical depth contributed by cirrus; it can be a factor of two or more for cirrus particles having effective radii in excess of 10 or 20 microns, for the 1.2° field-of-view of the AERONET Sun photometers [e.g., *Russell et al.*, 2004]. We examine in more detail the trends, and investigate likely causes, in the aerosol type-specific subsections that follow.

3.1. Biomass Burning Sites

[24] Figure 3 contains plots showing MISR-AERONET differences, plotted against AERONET-derived AOT at midvisible wavelengths, for the sites at which biomass burning particles are expected during their respective regional fire seasons. For tropical Northern Hemisphere sites, Banizoumbou, Ouagadougou, and Ilorin (shades of brown in Figure 3), the burning season is November to May, with a peak in December–January; these sites produce the highest AOT values in Figure 3a and most of those in Figure 3b. Biomass burning is expected between June and October at southern tropical sites: Alta Floresta, Belterra, Cuiaba-Miranda (shades of green in Figure 3), Mongu, and Skukuza (shades of blue); the peak in Africa typically occurs during June–July, and for Brazil, in August–September. To the degree that sampling allows, these sites reach their highest AOT values during the southern burning season, but other components cloud the picture; for example, desert dust may contribute to the high AOT at Banizoumbou during these months.

[25] Overall, the AOT differences are small (Table 5), and scatter fairly uniformly about zero. However, during the peak of the southern burning season, for example, MISR midvisible AOT values at the southern sites are skewed low (blue and green points, Figure 3c). Biomass burning par-

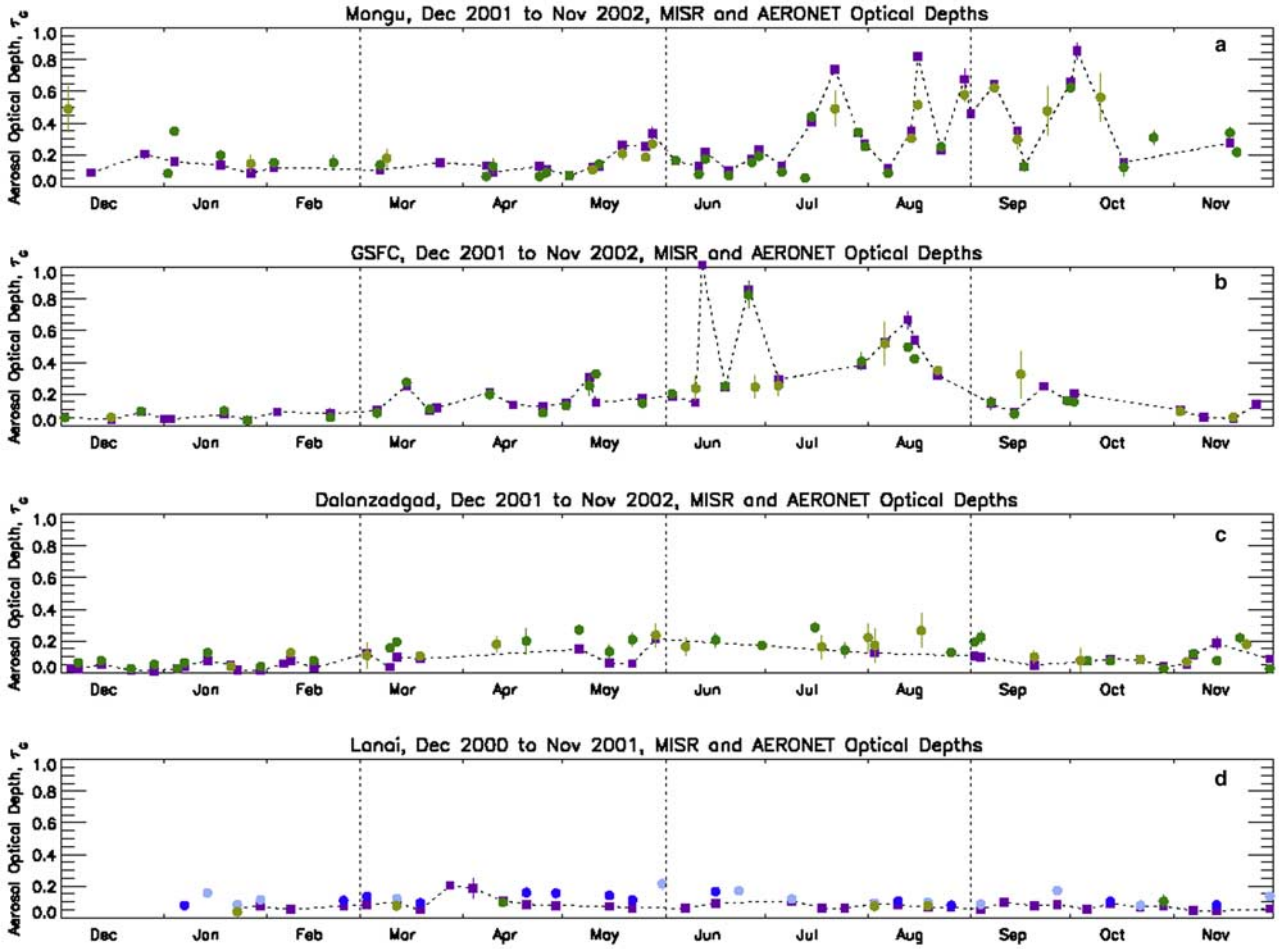

Figure 4. Yearlong green-band AOT time series plots for four representative cases, showing all successful aerosol retrievals, regardless of temporal coincidence, from AERONET (purple squares), MISR central land retrievals (dark green circles), MISR surroundings land retrievals (light green circles), MISR central ocean retrievals (dark blue circles), and MISR surroundings ocean retrievals (light blue circles). (a) Biomass burning site (Mongu, 2002). (b) Continental site (GSFC, 2002). (c) Dusty site (Dalanzadgad, 2002); Maritime site (Lanai, 2001). The AERONET observations are connected with dashed lines as a visual aid.

ticles are typically spherical, and mixtures of spherical particles in the early postlaunch MISR retrieval algorithm have SSA of 1.0 or 0.88 (Table 3). The more absorbing mixtures are picked frequently by the algorithm at these sites during June, July, and August (Table 4), and usually provide better agreement with AERONET AOT than nonabsorbing spheres. Recent field observations in southern Africa during the burning season find that biomass burning particles commonly have midvisible SSA around 0.84 [*Eck et al.*, 2003]. Other things being equal, higher AOT is required to match observed top-of-atmosphere reflectance as particle SSA decreases. This suggests that adding spherical particles having SSA near 0.84 to the algorithm climatology might bring the MISR results into even closer agreement with the Sun photometers for these situations. Also, in the medium, spherical particle category, the early postlaunch MISR aerosol algorithm contains only nonabsorbing particles. Spherical particle absorption is produced by externally mixing small black carbon particles (Table 2). Recent field data indicates that biomass burning would be better represented by internally mixing the absorbing material into medium-sized particles [*Eck et al.*, 2003; *Haywood et al.*, 2003].

[26] The data in Figure 3 also show several extreme outliers. At least a few of these are traced to scene variability. For example, the Banizoumbou observation on 14 June 2001 produced a MISR green band AOT over the central retrieval region of 0.794, compared with 0.217 from AERONET. However, the average of MISR retrievals in the eight surrounding regions was 0.562 ± 0.232. On this day, the AERONET midvisible AOT values ranged from about 0.2 to over 0.75, though in the 2-hour window of the MISR overpass, AOT at the Sun photometer site varied only by ±0.003. A similar situation applied on 17 August 2001, when the MISR AOT of 0.442 is compared with 0.219 from AERONET. In this case, the MISR surroundings retrievals produce AOT of 0.299 ± 0.122, and the AERONET AOT increased from about 0.2 to over 0.4 in the subsequent hours.

[27] Figure 4a is a time series plot showing all successful midvisible AOT retrievals, regardless of temporal coinci-

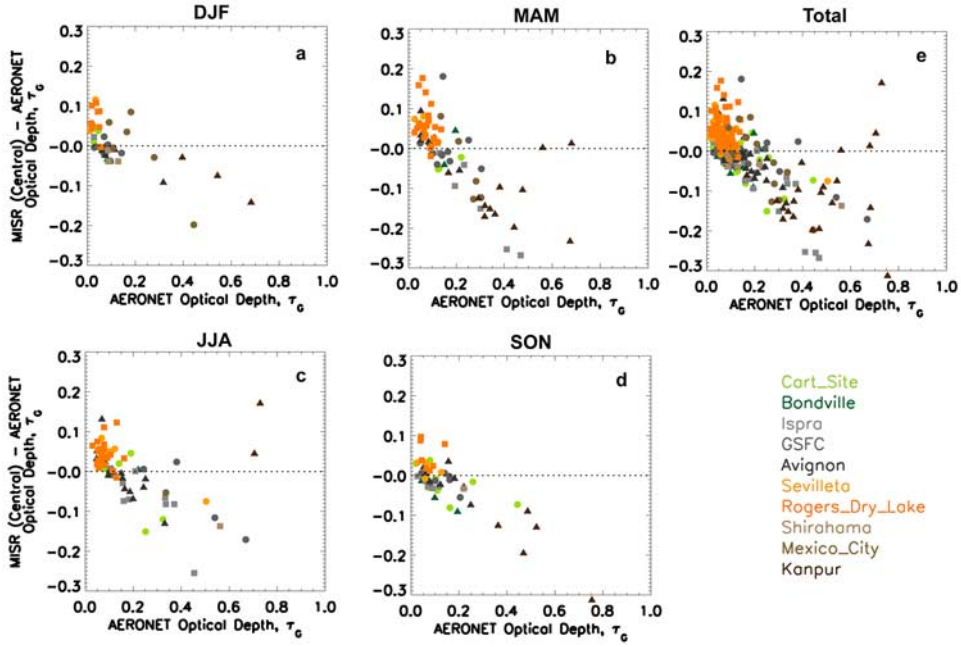

Figure 5. Same as Figure 3, but for 247 continental events. Rural sites are shown in shades of green; urban sites in grays, dusty sites in orange-yellow, and heavily polluted sites in browns.

dence, from AERONET, MISR (central), and MISR (surroundings), for Mongu, a representative biomass burning site. The similarity in mean values, relative magnitude of deviations, and climatological shift from background to burning season (July to early October) are all evident in this yearlong record.

3.2. Continental Sites

[28] The continental category covers a diversity of urban and industrial pollution aerosols, mixed to varying degrees with the other broad classes of aerosols, over a range of surface types. Pollution aerosols are primarily spheres, and the MISR algorithm rarely picks nonspherical dust particles at continental sites (Table 4); nearly all MISR retrievals in this category containing dust are for Rogers Dry Lake and Sevilleta in the southwestern United States (shown in shades of yellow in Figure 5); these sites have many attributes of desert.

[29] There is less seasonality in continental data than for the biomass burning and dusty categories. The primary pattern in MISR-AERONET AOT differences is a diagonal clustering of points that appears to have negative slope (Figure 5). The sharp edge to the lower left actually occurs in difference plots for all categories, but is most visible here due to the abundance of data points. Since MISR AOT values are constrained on physical grounds to be greater than zero, the MISR-AERONET AOT difference can be no smaller than the negative of the AERONET AOT. So points can not fall in the triangular region at the lower left of difference plots. (This attribute also diminishes the likelihood of extreme negative outliers, an asymmetry that appears throughout the MISR-AERONET comparison data set as well since we always plot the deviations versus AERONET rather than MISR AOT.) The exclusion zone in Figure 5 is larger than would be expected from this effect alone, in part because the MISR over land retrieval asserts a minimum AOT of 0.025, and in part because, as AOT increases, the likelihood of having a 100% AOT discrepancy decreases.

[30] The points comprising the clusters in Figure 5 are distinguished by site. The yellow subclusters, having AERONET AOT generally below 0.15, and residing primarily above the zero difference line, are from the desert-like Rogers Dry Lake and Sevilleta sites (see section 3.3).

[31] Gray and brown points dominate the tail of the data distribution. The brown points have AERONET AOT from about 0.15 to over 0.4, and represent measurements taken mainly at heavily polluted sites: Mexico City, Kanpur in northern India, and Shirahama in southern Japan. These sites are expected to have component particle SSA in the range of 0.8 to 0.85 [*Ramanathan et al.*, 2001; *Kahn et al.*, 2004]. The urban sites GSFC, Avignon, and Ispra create a scatter of gray points predominantly below the zero line, with AERONET AOT below about 0.3. These sites contribute to the low-MISR-relative-AOT tail most frequently in late spring and summer, when they experience episodes of heavy pollution (Figures 5b and 5c). An example is Ispra on 8 August 2001, when the MISR green band central AOT of 0.20 is compared to AERONET's 0.45 value. Scene variability is unlikely to account for the difference in this case; the MISR surroundings AOT values average to 0.25 ± 0.07, and the AERONET time series for the entire day extends upward from 0.45 to about 1.0. As discussed in section 3.1 for biomass burning cases, adding darker spherical particles to the MISR algorithm climatology could raise the retrieved AOT for these situations, and would better reflect observed particle properties under polluted conditions as well.

[32] The yearlong midvisible AOT time series for GSFC, a representative continental site, is shown in Figure 4b. It illustrates the overall agreement between the MISR and AERONET data sets, and to the degree severe AOT events

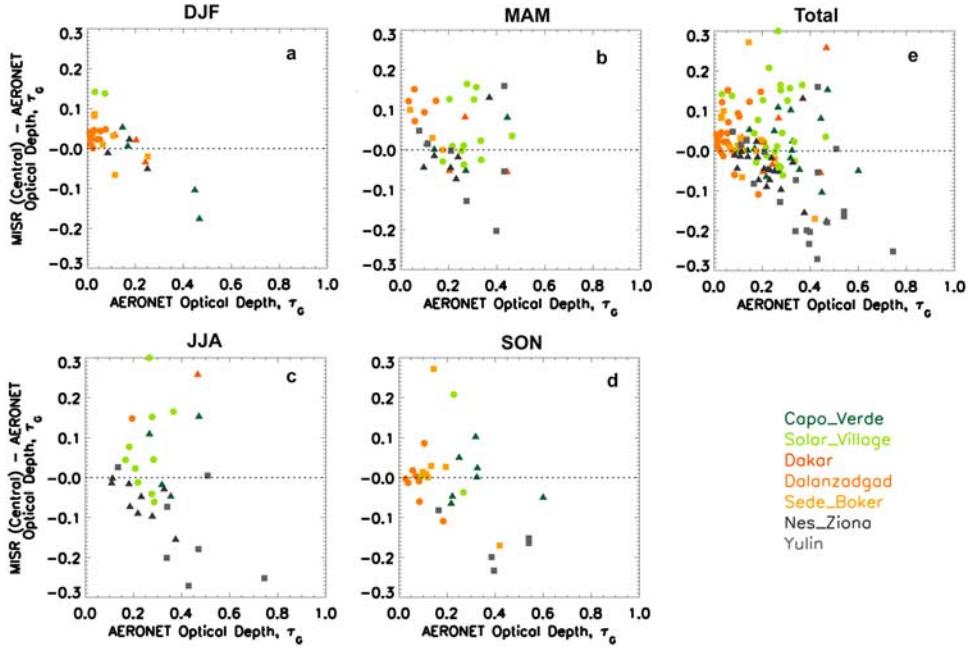

Figure 6. Same as Figure 3, but for 132 dusty events. Sites dominated by mineral dust are shown in yellow-orange shades, those that may often be dominated by pollution are shown in grays, and sites between the extremes are shown in green.

that occurred several times during the summer months are resolved by observations, the way each data record responds to such events.

3.3. Dusty Sites

[33] The quality of MISR aerosol retrievals over bright desert is documented by *Martonchik et al.* [2004]. Analyzing in detail observations from four sites during a 2-year period, they conclude that the MISR-retrieved AOT reliably falls within ±0.07 of coincident AERONET values. *Christopher and Wang* [2004] reach the same conclusion, for a single site in China. The present study covers a more diverse selection of seven sites at which dust is an important atmospheric aerosol component. For MISR-AERONET midvisible AOT differences, we obtain a standard deviation of 0.10 (Table 5). The sites examined here all reside in the Northern Hemisphere, where the dusty season extends from March or April into midsummer. Average AOT is comparable to biomass burning and continental cases, though the scatter in MISR (central)-AERONET AOT differences is higher than for other categories, and the correlation coefficient for the regression line is correspondingly lower. For some sites, such as Dalanzadgad and Dakar, the MISR-AERONET AOT differences are systematically high during the dustier spring and summer months (shown in orange and yellow shades in Figure 6), whereas for Yulin and Nes Ziona (shown in gray), they are systematically low, even during the dusty season.

[34] Several factors seem to be at play for these sites. First, the frequency with which the MISR algorithm best fitting aerosol mixture includes dust components is surprisingly low (Table 4), considering that at least over ocean, the multiangle radiances are very sensitive to particle sphericity [*Kahn et al.*, 1997]. Although sensitivity to particle shape could be lower over land sites, the lack of dust components chosen may be due to overly absorbing dust optical models in the early postlaunch MISR climatology, causing the operational algorithm to reject them when comparing with observations. The midvisible SSA is 0.88 for medium and 0.69 for coarse dust (Table 2), derived from measurements taken before 1980 that are no longer accepted as representative of airborne dust particles. When dust is a retrieved component with the current algorithm, the resulting AOT is usually skewed high, a further indication that the dust component SSA is too low. New nonspherical dust models that incorporate recent field campaign results for Asian and Saharan dust, having more realistic shapes and midvisible SSA around 0.97, are being incorporated into the MISR climatology, and seem to resolve these issues [*Kalashnikova et al.*, 2005].

[35] Both Nes Ziona and Yulin, the sites having systematically low MISR AOT, are near heavily populated areas that support industrial activity. At Yulin, for example, pollution is reported to dominate aerosol loading frequently [*Alfaro et al.*, 2003]. This accounts for the increased scatter between MISR and AERONET for dusty sites analyzed here, compared to the *Martonchik et al.* [2004] study, and could explain the low MISR AOT values, as discussed in section 3.2.

[36] Figure 4c shows the yearlong midvisible AOT time series for Dalanzadgad, a representative dusty site. This record demonstrates how the MISR AOT reproduces the trends in the AERONET values, but is usually higher, especially during the dusty spring and summer seasons, when the MISR algorithm most frequently picks the available nonspherical dust components.

3.4. Maritime Sites

[37] Figure 7 summarizes the MISR-AERONET green band AOT differences for maritime events. Relatively few

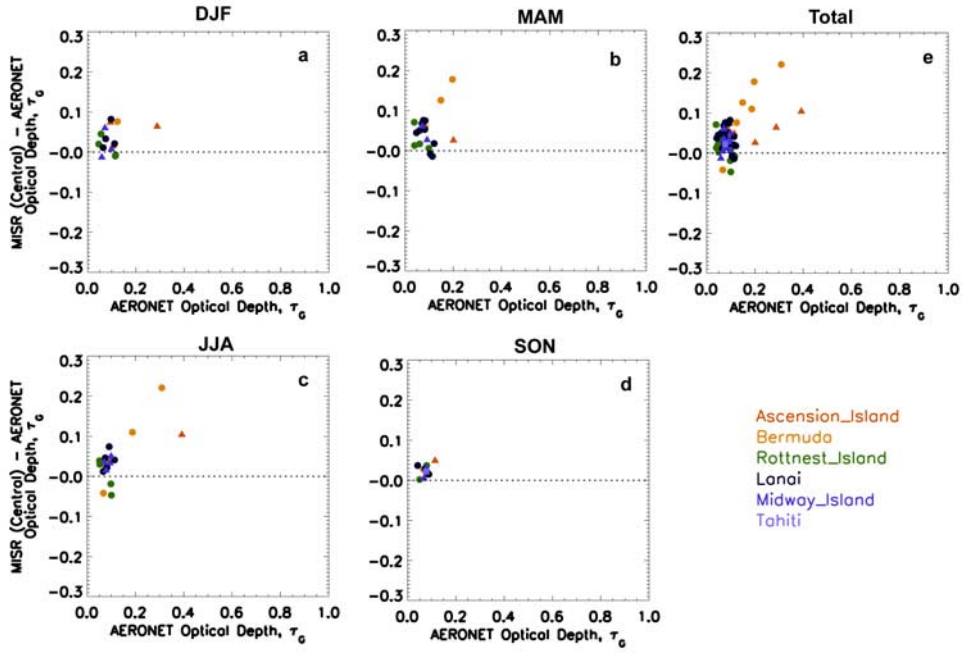

Figure 7. Same as Figure 3, but for 65 maritime events. The cleanest sites are shown in shades of blue, and the other sites are more frequently affected by transported pollution, runoff, or other factors.

AERONET stations qualify as maritime sites, and those having the best data records contain more gaps than the sites identified with land categories (Table 1). On a seasonal basis, maritime sampling in this data set is poor (Table 4), but overall, the MISR dark water AOT values are in even closer agreement with AERONET than the land ones, and outliers are smaller in magnitude. One pattern stands out in Figure 7: a small but persistent positive difference between MISR and AERONET retrieved values. This offset has also been noted in comparisons between coincident MISR and airborne Sun photometer measurements over dark water [*Redemann et al.*, 2005].

[38] For maritime cases, the MISR dark water aerosol retrieval algorithm is used, rather than the land retrieval algorithm. As long as the midvisible AOT is below 0.5, the early postlaunch dark water algorithm considers only the 18 red and near-infrared MISR channels, and relies on low ocean-surface reflectivity in these bands to reduce uncertainties associated with the treatment of light emanating from the lower boundary. Standard approaches are adopted for modeling surface Fresnel reflection, wind speed-dependent white caps, and Sun glint contributions, whereas the water-leaving radiance component in the red and near-infrared bands is assumed to be negligible [*Martonchik et al.*, 1998; *Kahn et al.*, 2001b]. (When AOT exceeds 0.5, the ocean surface is significantly obscured by aerosol, and the dark water retrieval algorithm adopts a procedure that incorporates additional information from the MISR blue and green bands.)

[39] The combination of low surface reflectance and typically low midocean aerosol loading creates top-of-atmosphere equivalent reflectances between 5% and 10% in midvisible, and as low as 1% in the near-infrared. Under these circumstances, errors of a few percent in MISR band-to-band, camera-to-camera, or absolute low-light-level calibration can have a significant impact on aerosol retrieval results. Calibration accuracy this stringent is at the cutting edge of current capabilities. Recent MISR team investigations using a range of calibration approaches resulted in spectral calibration adjustments of about 3% in the red band and 1% in the near-infrared [*Bruegge et al.*, 2004]. The version 12 aerosol products used in the present study were generated before the adjustments were incorporated into the MISR standard algorithms. When included, these changes alone reduce by as much as half the 0.05 average dark water AOT discrepancy with AERONET [*Kahn et al.*, 2005; *Abdou et al.*, 2005].

[40] The MISR algorithm's choice of aerosol component model may also contribute to the maritime AOT positive offset. MISR sensitivity to aerosol microphysical properties begins to diminish when AOT falls below about 0.15, as might be expected [*Kahn et al.*, 2001a]. In low-AOT situations over dark water, moderately absorbing spherical aerosol components are sometimes favored over nonabsorbing ones in the current algorithm (Table 4). AOT retrieval with the multiangle technique is generally less affected by small errors in assumed particle properties than multispectral methods [e.g., *Kahn et al.*, 1998]. However, if only nonabsorbing particles are present, and the algorithm selects absorbing ones, artificially high AOT will be retrieved. The size of this effect, and more generally, MISR sensitivity to aerosol SSA over dark water, will be assessed once low-light-level calibration uncertainties are fully characterized.

[41] Assumptions in the early postlaunch MISR algorithm related to modeling water-leaving radiance for the ocean boundary condition may contribute to the small positive offset as well. Although the algorithm accounts for the

white cap, Fresnel reflection, and glint components of surface reflection, it assumes the water-leaving radiance component, also called "underlight," is zero in the red and near-infrared bands. For clean ocean, this quantity is typically 0.002 and 0.0007 in the red and near-infrared, respectively, but the values increase when silt, phytoplankton, or other contaminants are present. Nonnegligible water-leaving radiance, which is common in some coastal waters, would brighten the top-of-atmosphere reflectance, and if unaccounted for by the algorithm, would be interpreted as additional aerosol. Water-leaving radiance is not likely to be uniformly high for most of the remote ocean sites at which the AOT offset is observed. MISR may be able to identify such situations and retrieve AOT more accurately; we are researching the possibility of an advanced ocean aerosol algorithm that retrieves surface reflectance along with aerosol properties, as is done by the current MISR over land aerosol algorithm.

[42] A climatology of near-surface wind speed drives the ocean surface white cap model in the early postlaunch MISR algorithm. According to the model, white caps become significant when the wind speed exceeds about 7 m/s. They boost the top-of-atmosphere radiance, and if not taken into account, will also produce MISR-retrieved AOT values that are too large. We expect the climatological wind data to be adequate for this application, except when unusually high winds occur under cloud-free conditions. Such events may be responsible for occasional, severe outliers, but seem unlikely to play a role in the systematic offset.

[43] Figure 4d shows MISR and AERONET green band AOT time series for a full year at Lanai, a representative maritime site. The MISR values track very closely those from AERONET, offset by approximately 0.05. As discussed above, we expect to reduce and possibly eliminate altogether this bias through instrument calibration adjustments, particle property updates, and possibly improvements to the treatment of ocean surface reflectance.

3.5. Spectral AOT and Aerosol Size Distribution

[44] We have compared up to this point only MISR-AERONET midvisible AOT, stratified by expected particle type. As discussed above, aerosol SSA, which is related primarily to particle chemical composition, probably makes the largest contribution to the midvisible AOT discrepancies, except for maritime cases. Patterns of mean AOT differences in Table 5 hint that there is additional information in spectral AOT comparisons. For all categories but maritime, the percent differences increase with increasing wavelength, because the AOT itself decreases with wavelength, making the ratio more sensitive to differences at longer wavelengths. By comparing MISR-retrieved AOT with airborne Sun photometer measurements, we used this relationship to determine that the prelaunch MISR algorithm was lacking small, nonabsorbing particles [*Schmid et al.*, 2003; *Martonchik et al.*, 2002].

[45] To quantify such comparisons, AOT spectral slope is often parameterized as the Angstrom exponent (A_λ), which can be defined as the negative slope of the least squares line fit to the logarithm of spectral AOT as a function of wavelength. For monomodal, lognormal aerosol size distributions, A_λ assumes values in excess of unity for typical medium-mode particles, and values below about 0.5 for coarse-mode aerosols.

[46] Figure 8 shows the mean MISR and AERONET spectral optical depths in each air mass type category, and A_λ for each data set is given in the figure legend. For the biomass burning and continental categories, the agreement is very close, well within the uncertainty expected based on temporal variability in the AERONET data and spatial variability in the MISR data alone. These distributions are dominated by medium-sized particles, as expected.

[47] For the dusty and especially the maritime categories, the MISR-derived A_λ is significantly larger than AERONET. Generally, this would suggest an overabundance of smaller particles in the aerosol properties retrieved by MISR. However, other factors are likely involved. For example, in nearly all the maritime cases, the MISR early postlaunch dark water retrieval was used. This algorithm considers data only in the red and near-infrared bands (see section 3.4), so where the MISR-AERONET maritime AOT discrepancies are largest, in the blue and green bands, the MISR AOT is extrapolated from aerosol optical models constrained at the longer wavelengths. Also, the actual magnitude of the discrepancy in the maritime curves is only about 0.05, comparable to the size of expected AOT changes due to low-light-level calibration adjustments [*Kahn et al.*, 2005].

[48] In dusty and maritime situations, significant contributions to the column AOT often come from both medium- and coarse-mode particles [e.g., *Dubovik et al.*, 2002]. Although the MISR early postlaunch algorithm climatology contains several bimodal mixtures having size distributions similar to those in the work of *Dubovik et al.* [2002] (Table 3, mixtures 9, 10, and the dusty mixtures), these mixtures represent a limited selection of medium- and coarse-mode relative abundance, and the only spherical particles involved are nonabsorbing. For example, A_λ for maritime cases ranges from 0.0 to 1.55 in the AERONET study, whereas for spherical, bimodal mixtures in the MISR early postlaunch climatology, the only available choices are 1.2 or 0.8 (Table 3).

[49] MISR is expected to have some sensitivity to bimodal and possibly even trimodal distributions, at least over dark water [*Kahn et al.*, 2001a]. A richer set of multimode particle mixtures than contained in the early postlaunch MISR algorithm climatology may be needed to adequately reproduce observed AOT spectral slopes, and to realize the full potential of the multiangle data. Testing in detail the results of multimodal retrievals will require additional ground-truth data not collected for the present study, such as AERONET sky-scan observations [*Dubovik and King*, 2000] since the Angstrom exponent alone cannot distinguish changes in component particle effective size from changes in the ratio of contributions from two or more aerosol components. Also, the data will need to be stratified so particle microphysical property differences within the broad categories treated here can be analyzed individually; this work is in progress.

4. Conclusions

[50] We quantitatively assessed the MISR early postlaunch AOT product, over land and ocean, by comparing

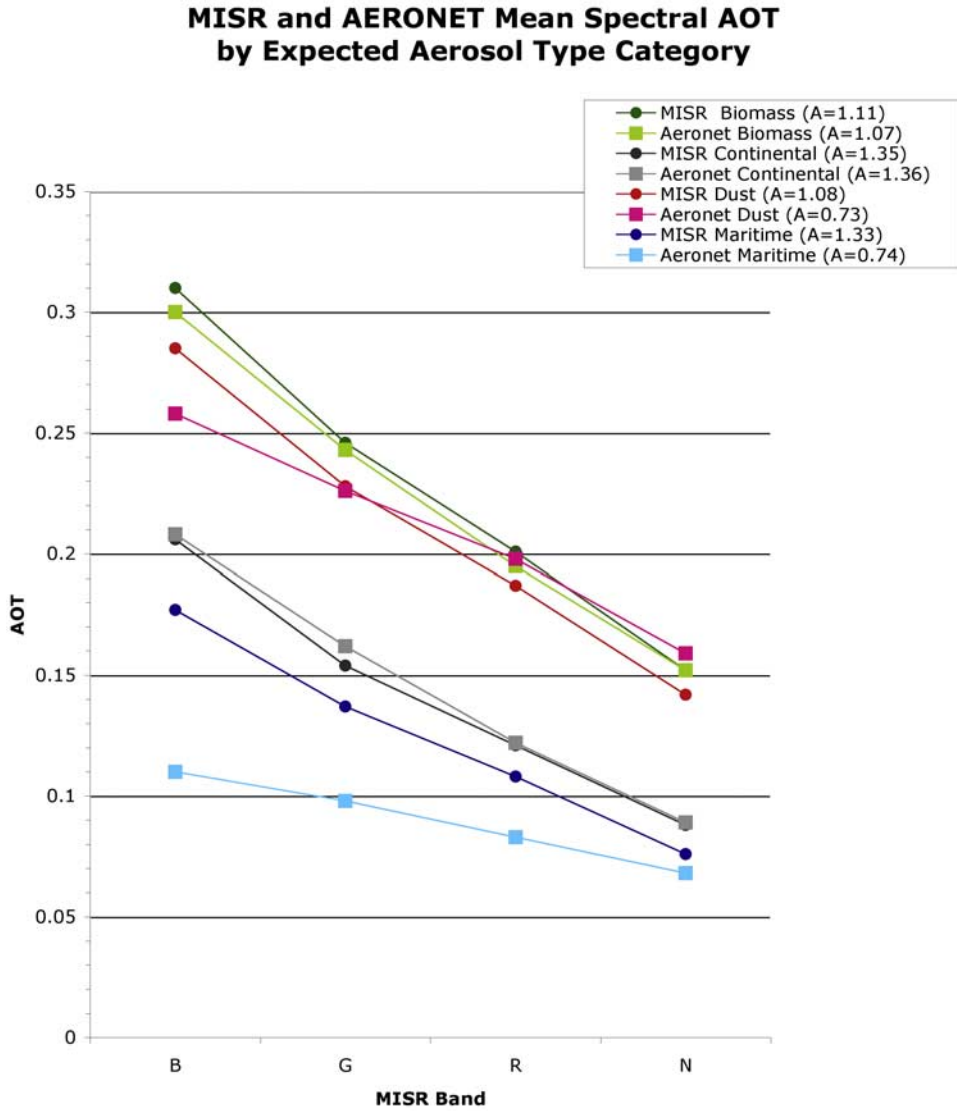

Figure 8. Mean MISR and AERONET spectral optical depths in each aerosol air mass type category for all central data points. Plotted symbols are connected with lines as a visual aid. The Angstrom exponents for each data set are given as "A" values in the figure legend.

with a 2-year measurement record of globally distributed AERONET Sun photometers. Our objectives were to provide uncertainty envelopes, and to identify likely causes for any discrepancies that might point toward ways of refining the algorithm.

[51] Several independent analyses demonstrate that MISR aerosol retrieval algorithm performance is already quite good compared with other remote sensing techniques, especially over bright surfaces [*Martonchik et al.*, 2004] and over land in general [*Abdou et al.*, 2005; *Liu et al.*, 2004]. In our study, overall, about 2/3 of the MISR-retrieved AOT values fall within [0.05 or 20% × AOT] of AERONET, and more than a third are within [0.03 or 10% × AOT] in all categories, a more comprehensive result that is consistent with other work. The MISR-retrieved spectral slopes for biomass burning and continental aerosol types are also in close agreement with Sun photometer values.

[52] We grouped together sites where biomass burning, continental, dusty, and maritime aerosols were thought to be dominant, and stratified the data in each group by season. As expected, uncertainties are smallest for maritime stations, and greatest for dusty sites. For example, the standard deviation of AOT differences is only 0.038 for green band maritime events; it is 0.071, 0.076, and 0.104 for biomass burning, continental, and dusty events, respectively (Table 5). Similarly, the correlation coefficient is 0.92 for midvisible maritime, 0.85, 0.87, and 0.73 for biomass burning, continental, and dusty cases. These results reflect in part that it is generally easier to retrieve from space the properties of bright aerosols over a dark water surface than over a bright desert or other land surface. Seventy-nine percent of the maritime central retrievals in this study were derived from the MISR aerosols-over-dark-water algorithm, whereas all the central retrievals in the biomass burning and continental categories, and 98% of the dusty cases, used the MISR aerosols-over-land algorithm.

[53] Detailed analysis of the patterns that emerged in the MISR-AERONET AOT differences suggests that adding to

the algorithm climatology spherical biomass burning and pollution aerosol analogs having lower SSA, and replacing existing ellipsoid dust models with more realistic, higher-albedo ones, would reduce the remaining discrepancies for MISR retrievals over land. Fine-tuning the instrument low-light-level calibration and possibly refining the algorithm's ocean surface model could reduce or eliminate a small but persistent offset in maritime AOT values. Also, the addition of a richer set of bimodal and possibly trimodal aerosol mixtures to the algorithm climatology seems likely to allow the aerosol retrieval algorithm to take advantage of additional information in the MISR data. In a few cases over land, where aerosol plumes are likely to occur, we were able to trace outliers to actual scene variability on 10-km scales; we expect that high-wind conditions over ocean may account for some outliers in the maritime data set.

[54] Assessing the quality of MISR-retrieved aerosol type, and re-evaluating AOT sensitivity for an upgraded algorithm, are the subjects of continuing work. On the basis of cases for which current particle models are representative, the second-generation MISR aerosol retrieval algorithm incorporating improvements identified here could reduce the discrepancies overall by at least half, providing AOT accuracy unprecedented for a spaceborne technique.

[55] **Acknowledgments.** We thank our colleagues on the Jet Propulsion Laboratory's MISR instrument team and at the NASA Langley Research Center's Atmospheric Sciences Data Center for their roles in producing the MISR data sets. We also thank the AERONET principal investigators for contributing to the global aerosol data base. This research is supported by the EOS-MISR instrument project, and by the Climate and Radiation Research and Analysis Program in the Earth Sciences Division of the National Aeronautics and Space Administration, under D. Anderson. This work is performed at the Jet Propulsion Laboratory, California Institute of Technology, under contract with NASA.

References

Abdou, W. A., D. J. Diner, J. V. Martonchik, C. J. Bruegge, R. A. Kahn, B. J. Gaitley, K. A. Crean, L. A. Remer, and B. Holben (2005), Comparison of coincident Multiangle Imaging Spectroradiometer and Moderate Resolution Imaging Spectroradiometer aerosol optical depths over land and ocean scenes containing Aerosol Robotic Network sites, *J. Geophys. Res.*, doi:10.1029/2004JD004693, in press.

Alfaro, S. C., et al. (2003), Chemical and optical characterization of aerosols measured in spring 2002 at the ACE-Asia supersite, Zhenbeitai, China, *J. Geophys. Res.*, *108*(D23), 8641, doi:10.1029/2002JD003214.

Anderson, T. L., R. L. Charlson, D. M. Winker, J. A. Ogren, and K. Holmen (2003), Mesoscale variations of tropospheric aerosols, *J. Atmos. Sci.*, *60*, 119–136.

Bruegge, C. J., W. A. Abdou, D. J. Diner, B. J. Gaitley, M. C. Helmlinger, R. A. Kahn, and J. V. Martonchik (2004), Validating the MISR radiometric scale for the ocean aerosol science communities, in *Post-Launch Calibration of Satellite Sensors*, edited by S. A. Morain and A. M. Budge, pp. 103–115. A.A. Balkema, Brookfield, Vt.

Chin, M., P. Ginoux, S. Kinne, O. Torres, B. N. Holben, B. N. Duncan, R. V. Martin, J. A. Logan, A. Higurashi, and T. Nakajima (2002), Tropospheric aerosol optical thickness from the GOCART model and comparisons with satellite and Sun photometer measurements, *J. Atmos. Sci.*, *59*, 461–483.

Christopher, S., and J. Wang (2004), Intercompason between multi-angle imaging spectroradiometer (MISR) and sunphotometer aerosol optical thickness in dust source regions of China, implications for satellite aerosol retrievals and radiative forcing calculations, *Tellus, Ser. B*, *56*, 451–456.

Diner, D. J., et al. (1998), Multiangle Imaging Spectroradiometer (MISR) description and experiment overview, *IEEE Trans. Geosci. Remote Sens.*, *36*, 1072–1087.

Diner, D. J., et al. (1999a), MISR level 2 aerosol retrieval algorithm theoretical basis, *Rep. D11400, Rev. D*, Jet Propul. Lab., Pasadena, Calif.

Diner, D. J., L. DiGirolamo, and E. E. Clothiaux (1999b), MISR level 1 cloud detection algorithm theoretical basis, *Rep. D13397, Rev. B*, Jet Propul. Lab., Pasadena, Calif.

Diner, D. J., W. A. Abdou, J. E. Conel, K. A. Crean, B. J. Gaitley, M. Helmlinger, R. A. Kahn, J. V. Martonchik, and S. H. Pilorz (2001), MISR aerosol retrievals over southern Africa during the SAFARI-2000 dry season campaign, *Geophys. Res. Lett.*, *28*, 3127–3130.

Dubovik, O., and M. D. King (2000), A flexible inversion algorithm for retrieval of aerosol optical properties from Sun and sky radiance measurements, *J. Geophys. Res.*, *105*, 20,673–20,696.

Dubovik, O., A. Smirnov, B. N. Holben, M. D. King, Y. J. Kaufman, T. F. Eck, and I. Slutsker (2000), Accuracy assessments of aerosol optical properties retrieved from Aerosol Robotic Network (AERONET) Sun and sky radiance measurements, *J. Geophys. Res.*, *105*, 9791–9806.

Dubovik, O., B. Holben, T. F. Eck, A. Smirnov, Y. J. Kaurman, M. E. King, D. Tanre, and I. Slutsker (2002), Variability of absorption and optical properties of key aerosol types observed in worldwide locations, *J. Atmos. Sci.*, *59*, 590–608.

Eck, T. F., et al. (2003), Variability of biomass burning aerosol optical characteristics in southern Africa during the SAFARI 2000 dry season campaign and a comparison of single scattering albedo estimates from radiometric measurements, *J. Geophys. Res.*, *108*(D13), 8477, doi:10.1029/2002JD002321.

Hansen, J., M. Sato, A. Lacis, and R. Ruedy (1997), The missing climate forcing, *Philos. Trans. R. Soc. London B*, *352*, 231–240.

Haywood, J., P. Francis, O. Dubovik, M. Glew, and B. Holben (2003), Comparison of aerosol size distributions, radiative properties, and optical depths determined by aircraft observations and Sun photometers during SAFARI 2000, *J. Geophys. Res.*, *108*(D13), 8471, doi:10.1029/2002JD002250.

Holben, B. N., et al. (1998), AERONET—A federated instrument network and data archive for aerosol characterization, *Remote Sens. Environ.*, *66*, 1–16.

Intergovernmental Panel on Climate Change (IPCC) (2001), *Climate Change 2001: The Scientific Basis*, edited by J. H. Houghton et al., 881 pp., Cambridge Univ. Press, New York.

Kahn, R., R. West, D. McDonald, B. Rheingans, and M. I. Mishchenko (1997), Sensitivity of multiangle remote sensing observations to aerosol sphericity, *J. Geophys. Res.*, *102*, 16,861–16,870.

Kahn, R., P. Banerjee, D. McDonald, and D. Diner (1998), Sensitivity of multiangle imaging to aerosol optical depth, and to pure-particle size distribution and composition over ocean, *J. Geophys. Res.*, *103*, 32,195–32,213.

Kahn, R., P. Banerjee, and D. McDonald (2001a), The sensitivity of multiangle imaging to natural mixtures of aerosols over ocean, *J. Geophys. Res.*, *106*, 18,219–18,238.

Kahn, R., P. Banerjee, D. McDonald, and J. Martonchik (2001b), Aerosol properties derived from aircraft multi-angle imaging over Monterey Bay, *J. Geophys. Res.*, *106*, 11,977–11,995.

Kahn, R., et al. (2004), Environmental snapshots from ACE-Asia, *J. Geophys. Res.*, *109*, D19S14, doi:10.1029/2003JD004339.

Kahn, R., et al. (2005), MISR low-light-level calibration, and implications for aerosol retrieval over dark water, *J. Atmos. Sci.*, in press.

Kalashnikova, O. V., R. Kahn, I. N. Sokolik, and W.-H. Li (2005), Ability of multiangle remote-sensing observations to identify and distinguish mineral dust types: 1. Optical models and retrievals of optically thick plumes, *J. Geophys. Res.*, doi:10.1029/2004JD004550, in press.

Liu, Y., J. A. Sarnat, B. A. Coull, P. Koutrakis, and D. J. Jacob (2004), Validation of Multiangle Imaging Spectroradiometer (MISR) aerosol optical thickness measurements using Aerosol Robotic Network (AERONET) observations over the contiguous United States, *J. Geophys. Res.*, *109*, D06205, doi:10.1029/2003JD003981.

Martonchik, J. V., D. J. Diner, R. Kahn, M. M. Verstraete, B. Pinty, H. R. Gordon, and T. P. Ackerman (1998), Techniques for the retrieval of aerosol properties over land and ocean using multiangle imaging, *IEEE Trans. Geosci. Remote Sens.*, *36*, 1212–1227.

Martonchik, J. V., D. J. Diner, K. Crean, and M. Bull (2002), Regional aerosol retrieval results from MISR, *IEEE Trans. Geosci. Remote Sens.*, *40*, 1520–1531.

Martonchik, J. V., D. J. Diner, R. Kahn, B. Gaitley, and B. N. Holben (2004), Comparison of MISR and AERONET aerosol optical depths over desert sites, *Geophys. Res. Lett.*, *31*, L16102, doi:10.1029/2004GL019807.

Mishchenko, M. I., L. Travis, R. Kahn, and R. West (1997), Modeling phase functions for dust-like tropospheric aerosols using a shape mixture of randomly oriented polydisperse spheroids, *J. Geophys. Res.*, *102*, 16,831–16,847.

Ramanathan, V., P. J. Crutzen, J. T. Kiehl, and D. Rosenfeld (2001), Aerosols, climate, and the hydrological cycle, *Science*, *294*, 2119–2124.

Redemann, J., B. Schmid, J. A. Eilers, R. Kahn, R. C. Levy, P. B. Russell, J. M. Livingston, P. V. Hobbs, W. L. Smith Jr., and B. N. Holben (2005), Suborbital measurements of spectral aerosol optical depth and its variability at sub-satellite-grid scales in support of CLAMS, 2001, *J. Atmos. Sci.*, in press.

Remer, L. A., et al. (2005), The MODIS aerosol algorithm, products and validation, *J. Atmos. Sci.*, in press.

Russell, P. B., J. M. Livingston, O. Dubovik, S. A. Ramirez, J. Wang, J. Redemann, B. Schmid, M. Box, and B. N. Holben (2004), Sunlight transmission through desert dust and marine aerosols: Diffuse light corrections to Sun photometry and pyrheliometry, *J. Geophys. Res.*, *109*, D08207, doi:10.1029/2003JD004292.

Schmid, B., et al. (2003), Coordinated airborne, spaceborne, and ground-based measurements of massive thick aerosol layers during the dry season in southern Africa, *J. Geophys. Res.*, *108*(D13), 8496, doi:10.1029/2002JD002297.

Smirnov, A., B. N. Holben, T. F. Eck, O. Dubovik, and I. Slutsker (2000), Cloud screening and quality control algorithms for the AERONET database, *Remote Sens. Environ.*, *73*, 337–349.

Tegen, I., P. Hollrig, M. Chin, I. Fung, D. Jacob, and J. Penner (1997), Contribution of different aerosol species to the global aerosol extinction optical thickness: Estimates from model results, *J. Geophys. Res.*, *102*(D20), 23,895–23,915.

Torres, O., P. K. Bhartia, J. R. Hermann, A. Syniuk, P. Ginoux, and B. Holben (2002), A long term record of aerosol optical depth from TOMS observations and comparison to AERONET measurements, *J. Atmos. Sci.*, *59*, 398–413.

Zhao, G., and L. Di Girolamo (2004), A cloud fraction versus view angle technique for automatic in-scene evaluation of the MISR cloud mask, *J. Appl. Meteorol.*, *43*, doi:10.1175/1520-0450, 860–869.

K. A. Crean, D. J. Diner, B. J. Gaitley, R. A. Kahn, and J. V. Martonchik, Jet Propulsion Laboratory, California Institute of Technology, 4800 Oak Grove Drive, Pasadena, CA 91109, USA. (ralph.kahn@jpl.nasa.gov)

B. Holben, NASA Goddard Space Flight Center, Greenbelt, MD 20771, USA.